Water film structure during rupture as revealed by MDS image analysis

Vu N.T. Truong [1], Liem X. Dang [2], Chen-luh Lin [1], Xuming Wang [1], Jan D. Miller [1]

[1] University of Utah, Department of Metallurgical Engineering, College of Mines and Earth Sciences, 135 South 1460 East, Rm 412, Salt Lake City, UT 84112

[2] Physical Sciences Division, Pacific Northwest National Laboratory, 902 Battelle Boulevard, Richland, WA 99352

Corresponding author: Jan.Miller@utah.edu (Jan D. Miller)

Abstract: The structure of thin water films during the rupture process was investigated by a new approach, which combines molecular dynamics simulation (MDS) with image processing analysis. The analysis procedure was developed to convert MDS trajectories to readable 3D images. The water films were studied at different thicknesses by MDS to determine the critical thickness at which the film ruptures. The potential energy of each specific film thickness during the simulation time was analyzed, and the results showed that the potential energy of stable films remained unchanged while the potential energy kept decreasing for films which ruptured during the simulation time. By applying the new procedure, the molecular porosity, which is defined as the void fraction between the volume of molecular pores in the water film and the total volume of the water film, was calculated. The results of molecular porosity for different film thicknesses during the simulation time suggested a critical molecular porosity of 49%. In other words, stable films have a molecular porosity of less than 49%. If a water film has a molecular porosity greater than 49%, rupture occurs during the simulation.

1. Introduction

Foam, a colloidal system of a dispersed gas phase and a continuous liquid phase, is widely used in our daily lives and for industrial fields such as mineral flotation, oil recovery, food processing and so on. The continuous liquid phase, generally water, forms a thin film between bubbles in the foam. The stability of foam and foam films is controlled primarily by the thinning and rupture of aqueous films between two bubbles. In the early stage of film thinning, the continuous aqueous phase drains out mostly due to the gravitational force. When the thickness of aqueous films decreases to a few hundred nanometers, the gravity effect can be negligible, and the stability of aqueous films is driven by physicochemical factors such as surfactant adsorption, film structure, intermolecular interactions (so-called disjoining pressure), and/or surface elasticity (Exerowa et al., 1981). In 1959, Scheludko and Mysels invented an experimental approach to measure single film thickness (Mysels, 1959; Scheludko and Exerowa, 1959). Subsequently, many experimental research studies have been accomplished by different research groups (Bergeron and Radke, 1992; Exerowa et al., 1987; Karakashev et al., 2008; Mishra et al., 2005; Schelero and von Klitzing, 2015; Yoon and Aksoy, 1999). Researchers have attempted to gain a better understanding of the properties of thin aqueous films, hence, critical parameters in film stability need to be determined.

In recent decades, the stability of thin aqueous films has been examined by the use of molecular dynamics simulation to obtain improved fundamental understanding at the nanometer scale. Using the Gromacs simulation program, Weng et al. studied the effect of film thickness on interfacial properties and found that the local surface tension distribution significantly varied with the film thickness, with a small variation in density profiles and surface tension values (Weng et al., 2000). Bhatt et al., for the first

time, calculated the disjoining pressure isotherm of free thin films from MD simulation results (Bhatt et al., 2002). Later on, Peng et al. proposed another method to compute the disjoining pressure from MD simulation results and also found that the temperature significantly affected the disjoining pressure isotherm (Peng et al., 2015). From another perspective, Yang et al. used MDS to investigate aqueous film rupture and determined the critical film thickness (Yang et al., 2009). The simulation conditions, including the film thickness and the simulation time, were examined. Peng et al. added the critical rupture time to the effect of ions on the film rupture process (Peng et al., 2012). A discrepancy of the aqueous film thickness between experimental work and simulation results is still reported in the literature; however, it is obvious that computational studies have contributed much information regarding the fundamental aspects of aqueous film properties.

Despite a number of research studies, molecular understanding of thin aqueous film stability is still incomplete, especially the film rupture process. In this paper, for the first time, the image processing approach was used in combination with MD simulations to provide new insight into film stability. Image processing has been widely used in recent decades in the fields of medicine, astronomy and mineral processing. Particularly in mineral processing applications, image processing has been used to investigate particle size, shape, density, porosity and pore network structures for multiphase systems (Fuerstenau and Han, 2003; Miller and Lin, 2009). In this study, image processing was applied to analyze the structure of molecular pores, defined as the void space between water molecules in aqueous films. It is expected that the molecular pore network significantly affects the rupture of a thin water film.

Our paper is organized as follows. First, MD simulation results for water films of different thickness are reported and the critical film thickness is established. The film rupture process is visualized and discussed. Second, the potential energy for water films of different thicknesses is studied during simulation time. Subsequent consideration of molecular porosity and percolation analysis from image processing was done in order to explain the film rupture process.

2. Computational approach

2.1 Molecular dynamics simulation

In this study, the simulation box was composed of a thin surfactant-free water film sandwiched between two vacuum spaces. To construct the desired size of a thin water film, GROMACS software was used, which enables the packing of water molecules with a density of close to 1 g/cc. Basically, thin films of 10 nm x 10 nm with different thickness were studied to determine the critical film thickness. The numbers of water molecules for each specific thickness are listed in Table 1. The thin water film was then centered in the simulation box's z direction. The simulation box size was 10 nm x 10 nm x 10 nm, and a periodic boundary condition was applied for the three directions.

Table 1. Number of water molecules assigned for each specific film thickness of 10 nm x 10 nm films by Gromacs software

Thickness (nm)	Number of water molecules
1.0	3,214
1.2	3,907
1.3	4,358
1.4	4,607
1.5	5,039
2.0	6,242

Amber 14 was used for the simulation of thin water films in this study. The total potential energy in the Amber program includes the Coulombic (electrostatic) interactions, the short-range interactions (van der Waals energy), and the bonded interactions as shown in Eq. 1. It is noted that the bonded terms include the bond stretch and angle bend energy that are represented in the water models as harmonic terms.

$$E_{total} = E_{Coulombic} + E_{vdW} + E_{bond} + E_{angle} \qquad (1)$$

Eq. 2 describes the Coulombic energy, in which the energy of the interaction is inversely proportional to the distance of separation r_{ij},

$$E_{Coulombic} = \frac{e^2}{4\pi \in_0} \sum_{i \neq j} \frac{q_i q_j}{r_{ij}} \tag{2}$$

where q_i and q_j are partial charges for atom i and atom j, e is the charge of an electron, ϵ_0 is the dielectric permittivity of a vacuum (8.85419 x 10^{-12} F/m).

The van der Waals energy, represented by the conventional Lennard-Jones (12-6) functions is shown in Eq. 3,

$$E_{vdW} = \sum_{i \neq j} \varepsilon_{ij} \left[\left(\frac{r_{m,ij}}{r_{ij}} \right)^{12} - \left(\frac{r_{m,ij}}{r_{ij}} \right)^{6} \right] \tag{3}$$

where ε_{ij} is the depth of the potential well, and $r_{m,ij}$ is the distance at which the potential reaches its minimum.

The Particle Mesh Ewald (PME) method was used to describe the Coulomb long-range interactions and a cutoff of 9 Å was applied for the Coulombic and van der Waals interactions. The extended simple point-charge (SPC/E) water model, which provides a good representation of the dielectric properties as well as the thermodynamic properties at a relatively low computational cost, was used for all the simulations of thin water films.

The thin water films were simulated in the NVT ensemble where the number of particles (N), the simulation box volume (V) and the temperature (T) were kept constant. The temperature was kept at 298.0 K using the Anderson thermostat. The energy of the system was initially minimized and equilibrated for 100 ps before the simulation. Simulations were carried out with a 2-fs time step, and the simulation time was varied up to the time at which film rupture occurred.

2.2 Conversion from MDS results to readable image processing formats

Basically, MDS results provide the trajectories of water molecules throughout the simulation time. However, image processing software is not able to read the format of Amber output trajectory files. Hence, a procedure to convert Amber output files to image processing readable files was developed as described in Fig. 1. It is noted that the Amber output file is a movie of trajectories which include a specific number of image frames up to the initial setting configuration. Since it was of interest to investigate the dynamics of water molecules during the simulation time, the trajectory of water molecules for 500 ps of simulation time was analyzed. As a result, a movie of trajectories was split into a series of coordinates in Amber. For analysis, a code written in C language was developed to create the digitized 3D image files, which are of readable format for the image processing software. To develop this code, the input files (called temporary input files in Fig. 1) required the information of the xyz coordinates, which were obtained from the MD simulations, and the radius of each atom. The concept is that each hydrogen atom or oxygen atom in a water molecule is considered to be a sphere with the van der Waals radius reported in the literature (Bondi, 1964). The van der Waals radii for oxygen and hydrogen atoms are 1.52 Å and 1.20 Å, respectively. A script was written to create the temporary input files, then the digitized 3D image files were finally made using the specific code.

2.3 Image processing

Image processing is a method used to convert an image into digital form and then proceed with the operations for analysis. Usually the input is the image and the output can be an image or the characteristics of an image. In this study, image processing software named ImageJ/Fiji was used to analyze the simulation results (Abràmoff et al., 2004). Of particular interest were the molecular pores during the rupture of the water film. In this regard, the molecular porosity was determined using ImageJ/Fiji. The computation procedure is shown in Fig. 2. At first, the digitized 3D image in raw file format was obtained from the conversion procedure as mentioned in Section 2.2, which is an 8-bit image with a 100 pixel x 100 pixel x 100 pixel configuration corresponding to 10 nm x 10 nm x 10 nm in

dimensions. Further, it was necessary to remove the slices of vacuum layers from these images in the simulation box, so the image analysis could be processed accurately. The images were inverted so the molecular pores between water molecules were taken into account for analysis. Fig. 3 shows an illustration of the original raw image and the inverted image. Before proceeding with molecular pore analysis using the 3D Object Counter, the inverted images were segmented by the Watershed function in ImageJ. It is worth noting that segmentation of the image is the separation process to identify objects of interest, which is an important part of image analysis.

Basically, the 3D Object Counter function provides the information of molecular pore volume in voxel units. In this way, the molecular pore volume during the simulation time was determined for different water film thicknesses. Further, the molecular porosity was computed using the similar concept of porosity in porous media. In other words, the molecular porosity is defined by the void fraction in Eq. (4). Thus, the molecular porosity can be found and evaluated at the point of water film rupture,

$$\phi = \frac{V_p}{V_t} \tag{4}$$

where V_p is the volume of molecular pores in the water film and V_t is the total volume of the water film.

Since the MDS results provided the trajectories of water molecules during the simulation time, a movie of water trajectories was achieved and split into a series of coordinate files in Amber simulation software, as discussed previously. Each coordinate file was converted into a 3D digitized image file, which was processed further to compute the molecular porosity. In other words, a series of coordinate files were required to be processed by the same procedure. For instance, a duration of 500 ps simulation time with 2 fs time-step provided a series of 250 coordinate files. To proceed with this procedure smoothly, a macro script was written in ImageJ/Fiji software to repeat the computation procedure for 250 coordinate files. As a result, the molecular porosity, as a function of simulation time, was obtained.
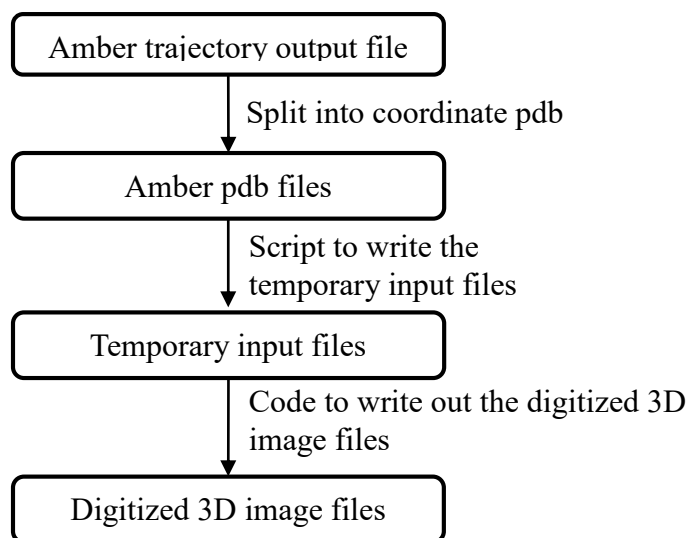
```
          ┌─────────────────────────────────┐
          │   Amber trajectory output file  │
          └─────────────────────────────────┘
                          │
                          ▼  Split into coordinate pdb
          ┌─────────────────────────────────┐
          │        Amber pdb files          │
          └─────────────────────────────────┘
                          │
                          ▼  Script to write the
                             temporary input files
          ┌─────────────────────────────────┐
          │      Temporary input files      │
          └─────────────────────────────────┘
                          │
                          ▼  Code to write out the digitized 3D
                             image files
          ┌─────────────────────────────────┐
          │     Digitized 3D image files    │
          └─────────────────────────────────┘
```

Fig. 1. Procedure to convert the Amber output trajectory files to the digitized 3D image files for image processing

3. Results and discussion

3.1 Critical water film thickness at nanometer scale

The critical film thickness is considered the thickness at which water film rupture occurs. In other words, the connectivity of void space (molecular pores) and rupture is not observed for thicker films and on this basis a critical thickness is defined. In this study, three values of the water film thickness were initially investigated including 1 nm, 1.5 nm and 2 nm. It is noted that the water film thickness is actually the initial thickness before MD simulation. It was observed that at 1 nm of thickness, the water film was broken after 500 ps of simulation time. Water films of 1.5 nm and 2 nm in thickness continued to run for an additional 10 ns to confirm the film stability. The film thicknesses in the range between 1 nm and 1.5

nm were later simulated with an increment of 0.1 nm. It was found that when starting from 1.4 nm for the water film thickness, the stability was sustained for longer simulation times. Therefore, the critical water film thickness was determined to be 1.3 nm. These simulation results are very similar to the reported studies of thin water films using different simulation software as shown in Table 2 (Jang and Goddard, 2006; Peng et al., 2012; Yang et al., 2009).
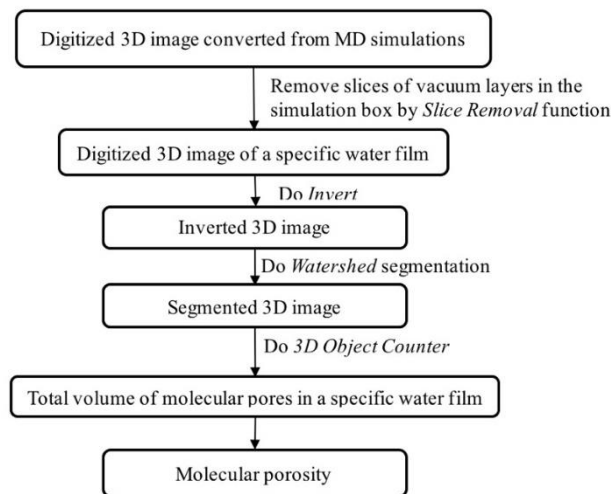

Fig. 2. Computation procedure for molecular porosity from 3D digitized image
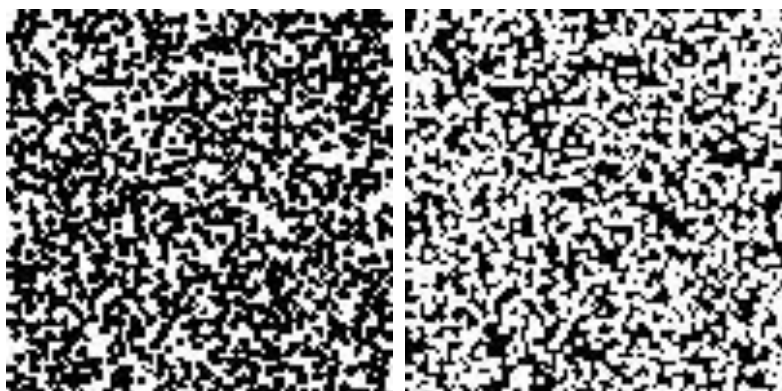
Fig. 3. Illustration of a slice of the original raw image (left image) and a slice of the inverted image (right image). Black spots in the left image are water molecules and black spots in the right image are molecular pores

Table 2. Simulation results for critical water film thickness as reported in literature and in this study

Film dimension	Critical Film Thickness	Reference
10 nm x 10 nm x 1.33 nm	1.33 nm	(Peng et al., 2012)
10 nm x 10 nm x 1.32 nm	1.32 nm	(Yang et al., 2009)
10 nm x 10 nm x 1.3 nm	1.30 nm	This study

Fig. 4 shows several snapshots from MDS results of the rupture process for the 1.30-nm water film. It was observed that the water trajectories created the low-density areas and high-density areas before a small hole for film rupture formed after about 110 ps of simulation time. This small hole grew to a larger size until the film broke into two separate pieces. Fig.5 shows snapshots of the water film before breaking into two specific water pieces. It was interesting to find that after the water film broke, it converted to the droplet state as shown in Fig. 6. It is noted that due to the periodic boundary condition of simulation, the real rupture process of a 1.30-nm water film is illustrated as seen in Fig. 5 and Fig. 6. The conversion of the broken film can possibly be explained by the lower potential energy of the droplet state. Due to the minimum surface area of the spherical droplet, the potential energy of the water droplet is reduced, so the thin water films tend to form water droplets after they are broken.
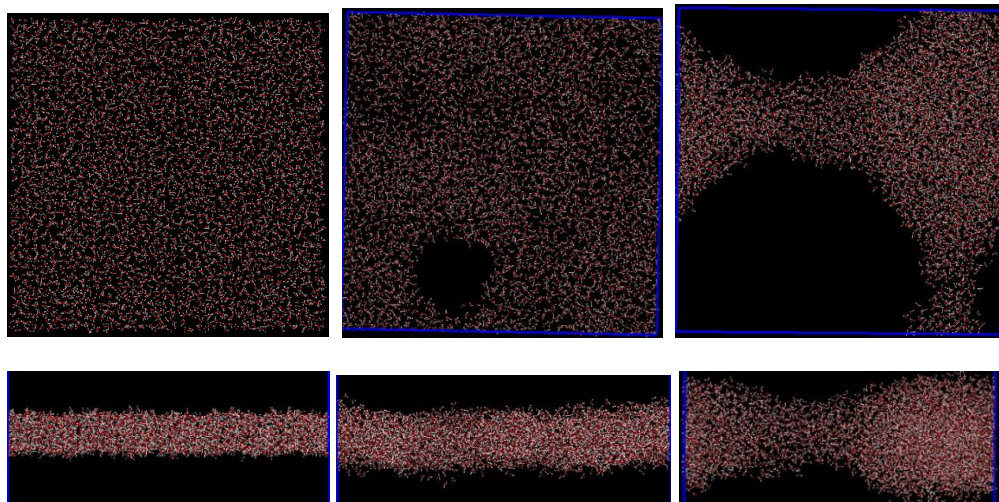
Fig. 4. The rupture process of a 1.30-nm water film. The left snapshots are the beginning state; the center snapshots are after 110 ps of simulation time; and the right snapshots are after 500 ps of simulation time. Top snapshots are the top view and bottom snapshots are the side view
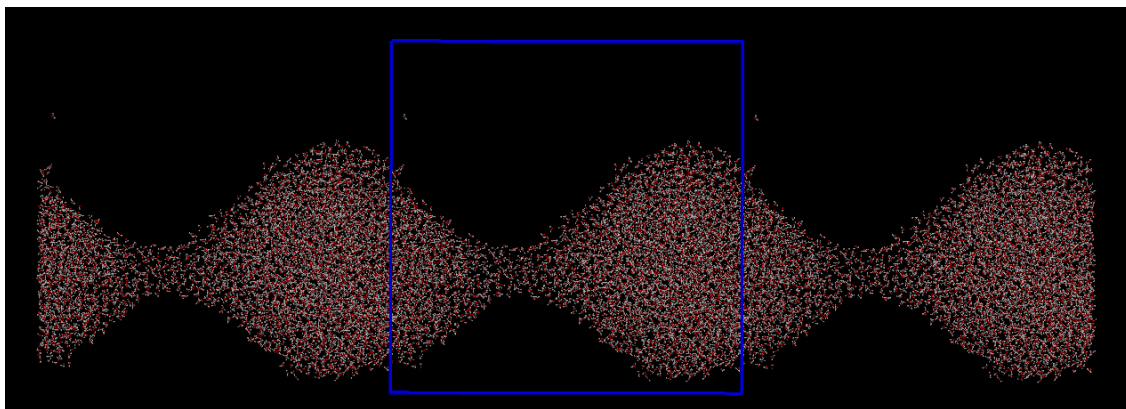

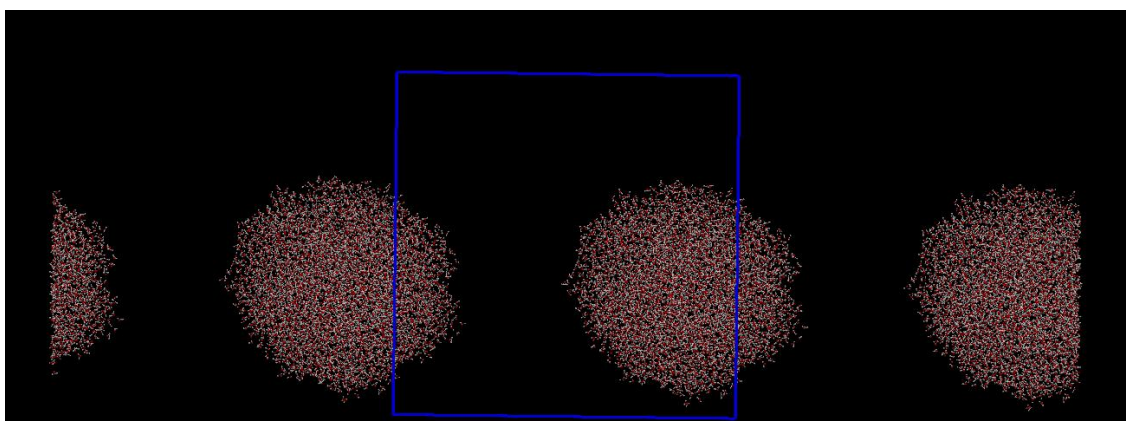Fig. 5. Snapshots of water film before breaking into two water pieces (the top view)

Fig. 6. Snapshots of droplet state after 1ns of simulation time for 1.30-nm water film (the top view)

3.2 Analysis of water film instability

3.2.1 Potential energy of the water film

To obtain better understanding of the water film rupture process, the potential energy of the water film as a function of simulation time was examined and the results are shown in Fig. 7. It can be seen that as for the stable films, the potential energy remained constant and just fluctuated around the equilibrium

values whereas the potential energy of broken films continued to decrease with an increase in simulation time. A slight decrease of potential energy was observed for the 1.30-nm water film and a dramatic decrease was observed for the 1-nm water film. The decrease of potential energy for these broken films occurred at the time when a small hole started to form inside the films as discussed in Section 3.1.

As introduced in Section 2.1, the total potential energy in the Amber simulation program consists of the Coulombic (electrostatics) interaction energy, the van der Waals interaction energy and the bonded energies (bond, angle and dihedral terms). Basically, in the simulation of surfactant-free water films, no bonded potential energy existed and just electrostatics and van der Waals interactions were reported. The decrease of potential energy in the broken films indicates that the electrostatic and van der Waals interactions between atoms become weaker throughout the simulation time, so film rupture occurred. As for the unbroken films, the stability was achieved probably because the electrostatics and van der Waals interactions between atoms remain constant and reach equilibrium during the simulation time. As expected, the analysis demonstrates that at the molecular level of understanding, the interactions between water molecules in a water film play an important role in film stability. This finding is in the good agreement with the experimental research of film stability with regard to the disjoining pressure and interaction forces in the thin film. Karakashev et al. reported the significant effect of DLVO disjoining pressure, in general, and the double-layer interaction, in particular, to film stability and film drainage (Karakashev et al., 2008).
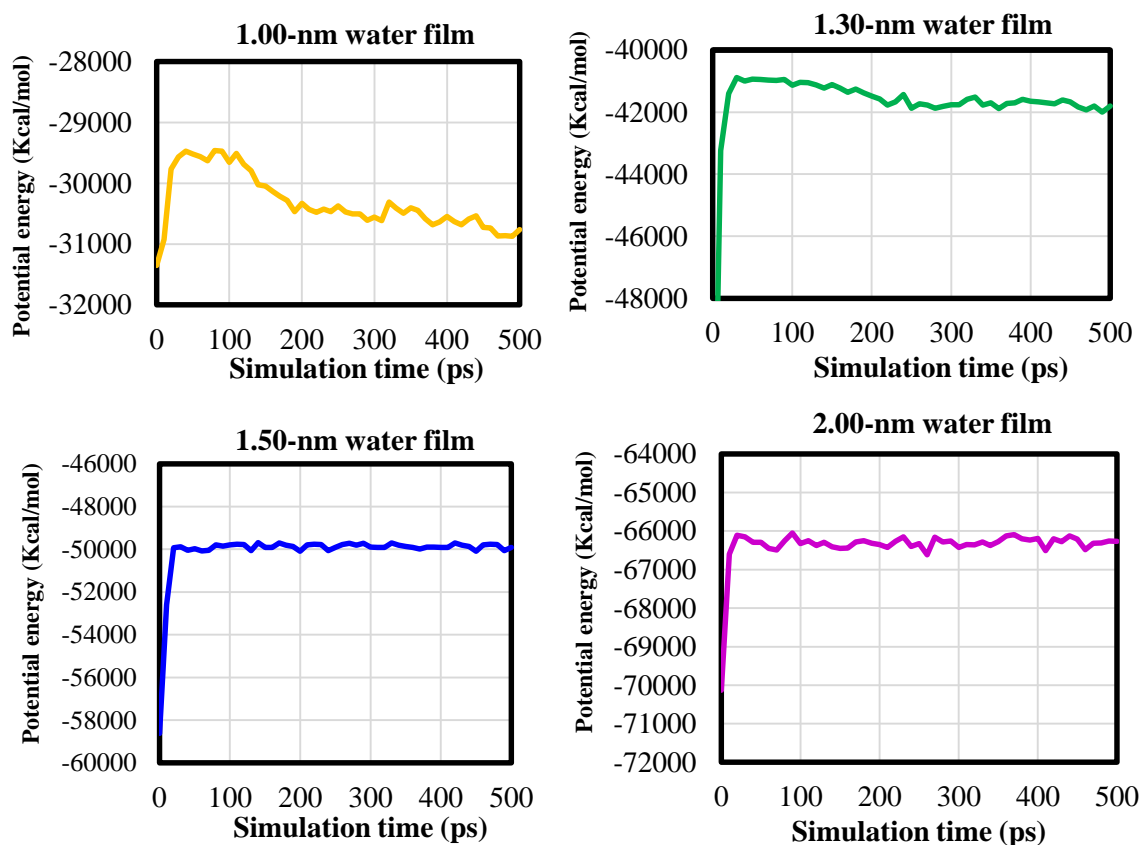

Fig. 7. Potential energy of water films at different thicknesses

3.2.2 Molecular porosity and percolation theory

In this section, the molecular porosity of a water film at specific thickness is examined further in order to explain film instability. It is worth noting that although the watershed segmentation was implemented to purposely separate the molecular pores in the water film, analysis results with the 3D Object Counter reveal that only one object could be detected. It means that all the molecular pores were connected and it was impossible to define the individual molecular pore size. Fig. 8 shows the molecular porosity of water films at different thicknesses as a function of simulation time. The results reveal that

the porosity of unbroken films remained unchanged during the simulation time whereas an increase in porosity was observed for the broken films. Further, from Fig. 8 the existence of a transition state for the broken films can be observed. This transition state was found from 110 ps to 300 ps for the 1.30-nm water film, and it was from 100 ps to 180 ps for the 1-nm water film. As mentioned in Section 3.1, the MDS results revealed that the 1.30-nm water film started to be unstable after about 110 ps of simulation time. On the other hand, the molecular porosity of the 1.30-nm water film gradually increased at about the same simulation time. A similar observation was noticed for the 1-nm water film, the molecular porosity dramatically increased after about 100 ps of simulation, which agreed with the MDS water trajectories. In other words, the molecular porosity of the water film can be a significant parameter of the film instability at the molecular level. In this regard, the connectivity of molecular pore networks may control the film rupture process.
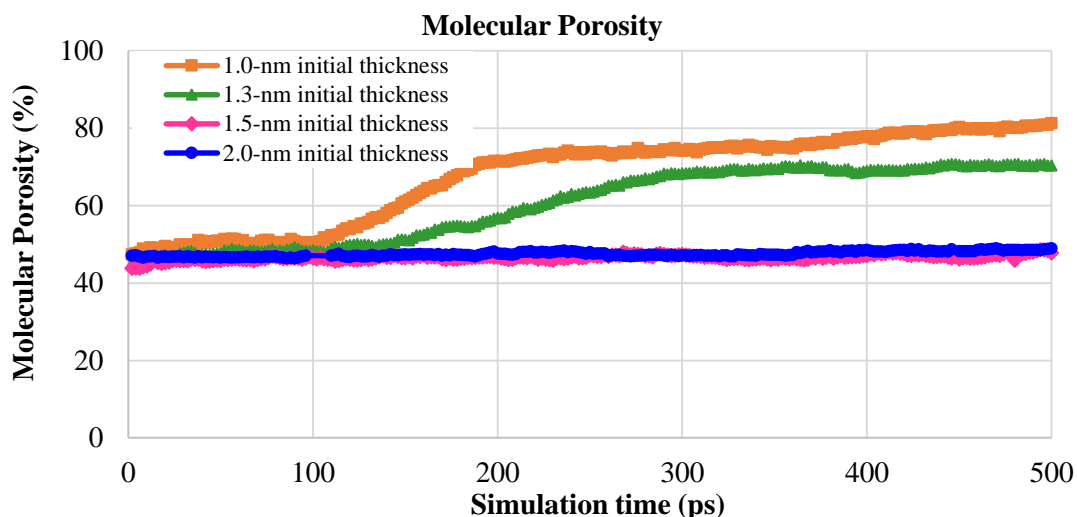

Fig. 8. Molecular porosity of water films at different initial film thicknesses as a function of simulation time

Table 3. Molecular porosity (percent) of water films at different thicknesses during 500 ps of simulation time

Simulation time (ps)	1-nm	1.3-nm	1.5-nm	2-nm
10	48.60	46.32	44.44	46.78
50	50.81	47.83	45.84	46.60
100	50.50	48.48	46.46	47.20
120	53.91	49.89	46.19	47.20
150	61.07	51.24	46.60	47.39
180	68.94	54.74	46.42	47.46
200	71.42	56.92	46.70	47.96
220	72.70	59.49	46.59	48.15
250	73.60	63.33	47.22	47.21
280	73.71	67.04	46.98	47.03
300	74.14	68.42	47.42	47.08
320	75.03	68.65	46.49	47.34
350	75.05	69.51	46.33	47.97
380	76.27	69.13	46.89	48.38
400	77.89	68.94	47.09	48.21
420	78.67	69.03	47.66	48.18
450	80.30	70.52	46.27	48.52
480	80.14	70.69	47.35	48.46
500	81.29	70.42	47.83	48.63

Table 3 provides the molecular porosity of different water films at selected simulation times. It can be seen that the stable films maintain molecular porosity of about 47 % ± 2%. The transition state can be defined from about 49 % ± 2 % to about 70 % ± 2 %, and the broken films have molecular porosity up to 80% ± 2 % after 500 ps of simulation time. Therefore, the critical molecular porosity can be determined to be about 49%. It means if the molecular porosity of a water film reaches 49% or above, film rupture can occur and film instability is expected. These data on the molecular porosity of water films together with the concept of the percolation theory can provide a better understanding of film rupture and film instability at the molecular level. In principle, concepts from the percolation theory should be appropriate to characterize the connectivity of preferred flow pathways (Jarvis et al., 2017; Renard and Allard, 2013). In this study, the flow pathways were considered as the pathways of molecular pores between water molecules and the percolation concept can be used to describe the connectivity of the molecular pore networks in water films. It is possibly expected that the molecular pores can percolate through the water film if the molecular porosity is larger than the critical value of 49%, as mentioned. Hence, film coalescence occurs.

4. Conclusions

Surfactant-free water films at different thicknesses were investigated by MD simulations to identify the critical thickness at which film rupture occurs, which was found to be 1.30 nm. This finding is in good agreement with values reported in the literature.

The potential energy of water films, which includes the van der Waals interaction and electrostatics interaction, were analyzed at different thicknesses by the compatible tool in the Amber program. Results revealed that within the super-thin nanometer scale of examined aqueous films, the potential energy of stable films remain unchanged during the simulation time, whereas a decreasing trend was found for broken films. This finding indicates that the interaction between water molecules in broken films was disturbed, so the film rupture occurred.

For the first time, percolation analysis following MD simulation was investigated to examine the connectivity of molecular pores in water films. As for the stable films, it was found that molecular porosity fluctuated around the equilibrium value and remained constant during the simulation time. On the other hand, the molecular porosity in the broken films kept increasing after a short time of stability. The critical value of the molecular porosity was defined as 49 %. It means that the molecular pore network can possibly percolate through the water film if the molecular porosity exceeds this critical value, hence, film rupture occurs.

Significantly the study of a surfactant-free water film by MD simulations reveals the fundamental understanding of the film rupture process at the molecular level. Also, the conversion procedure from MD trajectories to 3D images allows the application of an image processing tool for further analysis. It is expected that the percolation theory of molecular pores in water films can provide an important foundation for scientific research on thin film stability, hence, future work in this field can be achieved.

Acknowledgements

References

ABRÀMOFF, M.D., MAGALHÃES, P.J., RAM, S.J., 2004. *Image processing with ImageJ*. Biophotonics International 11, 36-42.

BERGERON, V., RADKE, C.J., 1992. E*quilibrium measurements of oscillatory disjoining pressures in aqueous foam films*. Langmuir 8, 3020-3026.

BHATT, D., NEWMAN, J., RADKE, C.J., 2002. *Molecular simulation of disjoining-pressure isotherms for free liquid, Lennard-Jones thin films*. The Journal of Physical Chemistry B 106, 6529-6537.

BONDI, A., 1964. v*an der Waals volumes and radii*. The Journal of Physical Chemistry 68, 441-451.

EXEROWA, D., NIKOLOV, A., ZACHARIEVA, M., 1981. *Common black and Newton film formation*. Journal of Colloid and Interface Science 81, 419-429.

EXEROWA, D., KOLAROV, T., KHRISTOV, K., 1987. *Direct measurement of disjoining pressure in black foam films*. I. *Films from an ionic surfactant*. Colloids and Surfaces 22, 161-169.

FUERSTENAU, M.C., HAN, K.N.,2003, *Principles of mineral processing*, SME, Littleton, CO, USA.

JANG, S.S., GODDARD, W.A., 2006. *Structures and properties of Newton black films characterized using molecular dynamics simulations*. The Journal of Physical Chemistry B 110, 7992-8001.

JARVIS, N., LARSBO, M., KOESTEL, J., 2017. *Connectivity and percolation of structural pore networks in a cultivated silt loam soil quantified by X-ray tomography*. Geoderma 287, 71-79.

KARAKASHEV, S.I., MANEV, E.D., NGUYEN, A.V., 2008. *Effect of double-layer repulsion on foam film drainage*. Colloids and Surfaces A: Physicochemical and Engineering Aspects 319, 34-42.

MILLER, J., LIN, C., 2009. *High resolution X-ray micro CT (HRXMT)–Advances in 3D particle characterization for mineral processing operations*. Recent Advances in Mineral Processing Plant Design, D. Malhotra, P.R.Taylor, E. Spiller and M. Levier. eds., SME, Littleton, CO, 48.

MISHRA, N.C., MURUGANATHAN, R.M., MÜLLER, H.J., KRUSTEV, R., 2005. T*he dependence of the interactions in foam films on surfactant concentration*. Colloids and Surfaces A: Physicochemical and Engineering Aspects 256, 77-83.

MYSELS, K.J., 1959. *Soap films: studies of their thinning and a bibliography*. Pergamon Press.

PENG, T., PENG, K., LI, Q., 2015. *Methodology for disjoining pressure of free water nanofilms*. The Journal of Physical Chemistry C 119, 14273-14280.

PENG, T.F., NGUYEN, A.V., PENG, H., DANG, L.X., 2012. *Quantitative analysis of aqueous nanofilm rupture by molecular dynamic simulation*. The Journal of Physical Chemistry B 116, 1035-1042.

RENARD, P., ALLARD, D., 2013. *Connectivity metrics for subsurface flow and transport*. Advances in Water Resources 51, 168-196.

SCHELERO, N., VON KLITZING, R., 2015. *Ion specific effects in foam films*. Current Opinion in Colloid & Interface Science 20, 124-129.

SCHELUDKO, A., EXEROWA, D., 1959. *Über den elektrostatischen Druck in Schaumfilmen aus wässerigen Elektrolytlösungen*. Colloid & Polymer Science 165, 148-151.

WENG, J.-G., PARK, S., LUKES, J.R., TIEN, C.-L., 2000. M*olecular dynamics investigation of thickness effect on liquid films*. The Journal of Chemical Physics 113, 5917-5923.

YANG, W., WU, R., KONG, B., ZHANG, X., YANG, X., 2009. *Molecular dynamics simulations of film rupture in water/surfactant systems*. The Journal of Physical Chemistry B 113, 8332-8338.

YOON, R.-H., AKSOY, B.S., 1999. *Hydrophobic forces in thin water films stabilized by dodecylammonium chloride*. Journal of Colloid & Interface Science 211, 1-10.